J Mater Sci: Mater Med (2010) 21:2751–2763
DOI 10.1007/s10856-010-4138-x

Preparation of superhydrophilic microrough titanium implant surfaces by alkali treatment

Stefano Tugulu · Konrad Löwe · Dieter Scharnweber · Falko Schlottig

Received: 20 January 2010 / Accepted: 26 July 2010 / Published online: 20 August 2010

Abstract A new strategy to render intrinsically hydrophobic microrough titanium implant surfaces superhydrophilic is reported, which is based on a rapid treatment with diluted aqueous sodium hydroxide solutions. The physicochemical characterization and protein interaction of the resulting superhydrophilic implant surfaces are presented. The superhydrophilicity of alkali treated microrough titanium substrates was mainly attributed to deprotonation and ion exchange processes in combination with a strong enhancement of wettability due to the roughness of the used substrates. Albeit these minor and mostly reversible chemical changes qualitative and quantitative differences between the protein adsorption on untreated and alkali treated microrough titanium substrates were detected. These differences in protein adsorption might account for the enhanced osseointegrative potential of superhydrophilic alkali treated microrough implant surfaces. The presented alkali treatment protocol represents a new clinically applicable route to superhydrophilic microrough titanium substrates by rendering the implant surface superhydrophilic "in situ of implantation".

1 Introduction

The term osseointegration describes the highly desired establishment of a direct structural and functional contact between an endosseous implant and bone [1, 2]. Due to its mechanical and chemical properties commercially pure titanium (Ti) is currently the material of choice for successfully osseointegrated implants [3]. Recent findings however indicate that the osseointegrative potential of Ti implants can be further enhanced by modifying their topographical and physicochemical surface properties [4] and various surface modification processes for Ti implants have been elaborated [5].

Microroughening of Ti implant surfaces, e.g., was reported to increase the bone to implant contact (BIC) as well as the removal torque forces in vivo [6, 7]. While this increase of removal torque forces might be mainly attributed to a better mechanical interlocking of rough implant surfaces with surrounding bone [8] the increased BIC values indicate that surface topography and roughness might also directly enhance bone healing and osteogenesis [9]. The enhanced proliferation, differentiation and matrix production of osteogenic cells that have been observed on microroughened implant surfaces in vitro support this hypothesis [10, 11].

Additionally to topography the physicochemical properties of the implant surface as surface charge, energy and hydrophilicity do also affect osseointegration [12]. Here, primarily biochemical and cell physiological processes as well as the nucleating and mineralizing ability of the implant surface might be affected by these properties [4, 13]. More specifically the surface energy of the implant surface was reported to affect cell response in vitro and osseointegration in vivo [14–17]. On the other hand, the (physico)-chemical surface properties of the implant were also discussed to influence "bone bonding", i.e., the formation of a direct chemical connection between the implant and bone mineral [18–20].

Furthermore, the physicochemical surface properties of a substrate might be crucial for the comprehension of the

S. Tugulu (✉) · F. Schlottig
Thommen Medical AG, Headquarters, Hauptstr. 26d, 4437 Waldenburg, Switzerland
e-mail: Stefano.tugulu@thommenmedical.com

K. Löwe · D. Scharnweber
Max Bergmann Center of Biomaterials, Technische Universität Dresden, Budapester Str. 27, 01069 Dresden, Germany

effect of surface topography on cell behavior in vitro and in vivo as, e.g., during wound healing and osteogenesis. This seems reasonable since the topography of the implant surface is detected by cells via transmembrane receptors that bind to an adsorbed layer of plasma proteins [21, 22]. The homogeneity, conformational status, composition and dynamics of this protein layer on the other hand is supposed to directly depend on the physicochemical properties of the substrate surface [23, 24].

Under physiological conditions the physicochemical surface properties of native Ti are determined by a thin passivation layer of TiO_{2-x}, which has been regarded to be compatible with proteins in their native conformation and with bone mineral [3, 25, 26]. Without specific storage conditions this TiO_{2-x} layer is however rapidly contaminated by the adsorption of hydrocarbons from the environment, which render microrough Ti substrates hydrophobic and repellent to water or tissue fluids with water contact angles of 130–140° [27, 28]. The adsorption of hydrocarbons has further been discussed to alter the osseointegrative potential of Ti implants [15, 16, 27–30]. As a result numerous techniques have been introduced to avoid or reduce hydrocarbon contamination on Ti implants and to enhance their wettability [18, 27, 31–36]. However these techniques are either technically demanding, time consuming or use harsh chemical reaction conditions, which might even interfere with the intended use of the resulting substrates in clinical implantology.

Recently we have presented the application of a mild alkali treatment to prepare superhydrophilic microrough commercial dental Ti implants with enhanced osseointegrative potential [37, 38]. Specifically sandblasted and thermal acid etched (SBA) Ti implant surfaces were treated with an aqueous 0.05 M NaOH solution by shaking or sonicating to overcome the initial wetting barrier.

Here, we present the detailed physicochemical characterization of the resulting alkali treated SBA Ti surfaces. The contributions of surface roughness and surface chemistry to the changes in wettability of the substrates were evaluated by determining the physicochemical and surface analytical properties of Ti substrates as a function of surface roughness and chemical surface treatment. Fibrinogen adsorption on SBA Ti substrates as a function of alkali treatment was further analyzed to discuss the enhanced osseointegrative potential of alkali treated microrough Ti substrates.

2 Materials and methods

2.1 Materials

Three types of Ti substrate geometries were used. All substrates consisted of titanium grade 4 (Dynamet Incorporated Washington). Substrates were cylindrically shaped (5 mm diameter and 15 mm height, modified with a drilled thread for fixation with the measurement equipment) or disk-shaped (15 mm diameter and 2 mm thickness). Additionally commercially available titanium Implants (SPI®ELEMENT and SPI®CONTACT, Thommen Medical AG, Switzerland) with a sandblasted, thermal acid etched surface (see below) were used.

Aqueous 0.1 M NaOH solution, 0.1 M HCl solution, NaCl, p.A., Na_2CO_3, p.A and NaOH, p.A. were obtained from Fluka, Switzerland and were diluted with or dissolved in deionized water (18.2 MΩ cm) prepared by an ELGA PURELAB Plus UV/UF purification system. Fibrinogen from human plasma Alexa Fluor 546 conjugate was obtained from Invitrogen. Round glass cover slips were obtained from Carl Roth GmbH, Karlsruhe, Germany and were rinsed with deionized water and isopropanol and subsequently dried in a stream of nitrogen before use.

2.2 Surface treatment

Surface treatment of Ti substrates consisted of machining (M), machining and subsequently sandblasting (SB) or of a sequence of machining, sandblasting and thermal acid etching (SBA). Sandblasting was carried out using Al_2O_3 particles of mean grain size of 125 μm. Thermal acid etching of sandblasted substrates was carried out in a mixture of 50% HCl (32%), 25% H_2SO_4 (95–97%) and 25% deionized water (v/v/v) and was followed by passivation in a mixture of 30% nitric acid (65–70%) and deionized water. M and SB substrates were used without this passivation.

Alkali treatment was performed at room temperature by sonicating the substrates in 0.05 M aqueous NaOH solution for 30 s or fixing and vigorously shaking the substrates in a vial filled with 0.05 M aqueous NaOH solution until the substrates were completely wetted. If mentioned the substrates were rinsed with deionized water directly after the alkali treatment.

2.3 Stereo scanning electron microscopy and calculation of roughness parameters

Stereo scanning electron microscopic (Stereo-SEM) measurements were carried out using cylindrically shaped, gold sputtered substrates using a Zeiss EVO25 (Zeiss, Germany) using SEM projections with a tilt angle variation of 6° at 800-fold magnification. 3D images of the surface topography were calculated using MeX V5.1 software (Alicona, Grambach, Austria). 3D-wavelength dependent roughness measurement was applied using the common cut-off method [39, 40]. Areal roughness parameters S_a (arithmetic mean of the surface points from the mean plane), S_q (root mean

square of the surface departures from the mean plane), S_{dr} (ratio of excess actual surface over the projected surface) and r (Wenzel roughness, i.e., ratio of the actual surface over the projected surface) values were calculated using a Gaussian filter with a cut-off wavelength $\lambda_c = 31$ μm [16]. Areas of 340 × 250 μm were used for evaluation.

2.4 Dynamic water contact angle measurements (DCA)

Advancing and receding water contact angles were measured by the dynamic Wilhelmy method on a KRÜSS K100 tensiometer (Krüss GmbH, Germany) using an immersion and emersion speed of 10 mm/min on cylindrical model substrates described above and by using deionized water as testing liquid [27]. Measurements were carried out as double measurements using 10 immersion and emersion cycles per sample. Reported values correspond to mean values that were derived from the first immersion/emersion cycle. Substrates were dried under a stream of nitrogen directly before the measurements.

2.5 X-ray photoelectron spectroscopy (XPS)

XPS measurements were carried out at Robert Mathys Foundation (Bettlach, Switzerland) on a Kratos Axis Nova (Kratos Analytical, Manchester, UK) using monochromatic AlK_α radiation (1486.7 eV) on disk-shaped substrates. Two disks were analyzed per measurement. On each disk 2 measurements with a probing area of 700 × 300 μm were carried out. The spectra were recorded in constant analyzer energy mode with 40 eV pass energy and a resolution of 0.15 eV. Small peak shifts were corrected by calibrating the aliphatic carbon signal to 285 eV as reference value. Chemical compositions were calculated by subtracting an iterated Shirley background from the curves and by using sensitivity factors provided by Kratos.

Fitting of high resolution spectra, peak attribution and selection of full width at half maximum (FWHM) values were carried out according to McCafferty et al. [41]. Reported values correspond to uncorrected mean values and the standard deviation.

Data obtained on flat disk-shaped substrates were confirmed by analysis of commercially available implants at Tascon GmbH (Münster, Germany) on a PHI Quantera SXP (PHI, Physical electronics, Chanhassen, USA) as double measurements using a probing area of 200 μm^2 and monochromatic AlK_α radiation.

2.6 Time-of-flight secondary ion mass spectrometry (TOF-SIMS)

Time-of-flight secondary ion mass spectrometry (TOF-SIMS) measurements were carried out at Tascon GmbH (Münster, Germany) on a TOF-SIMS IV (ION-TOF GmbH, Münster Germany) using Bi_1^+ as primary ion with a kinetic energy of 25 keV and 0.5 pA as primary ion current on commercially available implants. Probing area and time were 100 × 100 μm and 100 s, respectively. Alkali treated samples were allowed to dry at ambient atmosphere for 30 min before the measurements.

2.7 pH-measurements

Reported pH values were measured using a flat-membrane microelectrode (LoT403-M8-S7/120 Mettler Toledo) with 10 μl of freshly prepared isotonic NaCl solution as contact medium between the microelectrode and disk-shaped substrates. Values were recorded 5 min after bringing the substrates into contact with the microelectrode.

2.8 Protein adsorption

For the protein adsorption experiments SBA substrates were alkali treated by immersing half of the substrates in a 0.05 M NaOH solution. To facilitate wetting of the substrates ultrasound was applied. Residual solution was carefully removed from the substrates by using a lint free cleaning wipe and the substrates were dried in a stream of nitrogen.

1 μM fibrinogen Alexa Fluor 546 conjugate solution was prepared according to the manufacturer's instructions in 0.1 M Na_2CO_3-buffer of pH 8.3 and was directly used. Protein adsorption experiments were carried out as sandwich assay by incubating 20–40 μl of the protein solution between disk shaped SBA Ti substrates and round microscopy glass cover slips with 12 mm diameter for 5 min at room temperature in a glass chamber of saturated humidity in the dark. Substrates were subsequently washed 3× for 5 min with 0.1 M Na_2CO_3-buffer of pH 8.3, rinsed with deionized water and dried in a stream of nitrogen. Substrates were analyzed using a Tecan LS 200 laser fluorescence scanner with excitation wavelength of 543 nm and a cut of filter of 590 nm for detection. The optical resolution was 4 μm.

3 Results

3.1 Influence of surface topography and chemical treatment on the wetting of Ti substrates

The influence of surface topography and surface chemistry on the wettability of Ti substrates was assessed by combining Stereo-SEM and DCA measurements. Specifically the influence of surface energy was assessed by measuring the advancing water contact angles on machined (M),

sandblasted (SB), and sandblasted and thermal acid etched (SBA) substrates in three different chemical states, i.e., untreated, alkali treated with aqueous 0.05 M sodium hydroxide solution as well as alkali treated and rinsed with deionized water (rinsed). The latter group was used to test, if the increased wettability of alkali treated substrates was permanent or only temporary and due to the deposition of sodium and hydroxide ions on the substrate surface. The resulting changes in the wettability of individually structured substrates were evaluated in the context of qualitative surface topography and quantitative roughness parameters S_a, S_q, S_{dr}, and r of the surfaces as derived by Stereo-SEM.

As evidenced by top view electronmicrographs and calculated pseudo colored topographical 3D images of M, SB, and SBA Ti substrates in Fig. 1 and derived roughness parameters in Table 1 each substrate type showed individual features that were characteristic for the individual surface treatment. M substrates showed characteristic striations and grooves with submicron depth as exclusive topographical feature. S_a and r values of the M substrate were 0.25 μm and 1.12. Sandblasting by contrast generated a macrorough surface with cavities of irregular shape with a depth of up to 15 μm and with diameters of 10–50 μm. S_a and r values of the SB surface were 1.24 μm and 1.48, respectively. As evidenced by the electronmicrographs in Fig. 1 Al_2O_3 particles partly remained entrapped in the SB Ti surface. Stereo-SEM evidenced a hierarchical surface topography for the SBA substrates. Here, a macroroughness that was comparable to the one of SB substrates was combined with an additional "microroughness" with periodic microcavities with diameters of 1–2 μm. S_a and r values of the SBA substrates were 1.18 μm and 1.56, respectively. The decrease of S_a values from SB to SBA substrates might be attributed to a slight flatting of the macroroughness of the surface due to the ablation of material during the etching procedure. The SEM pictures of SBA Ti substrates further

Table 1 Areal roughness parameters of M, SB, and SBA Ti substrates as derived from stereo scanning electron microscopy

Modification	S_a (μm)	S_q (μm)	S_{dr} (%)	r
Machined (M)	0.25	0.31	12	1.12
Sand-blasted (SB)	1.24	1.58	48	1.48
Sandblasted acid etched (SBA)	1.18	1.57	56	1.56

S_a arithmetic mean of the surface points from the mean plane, S_q root mean square of the surface departures from the mean plane, S_{dr} ratio of excess actual surface over the projected surface, r Wenzel roughness, i.e., ratio of the actual surface over the projected surface

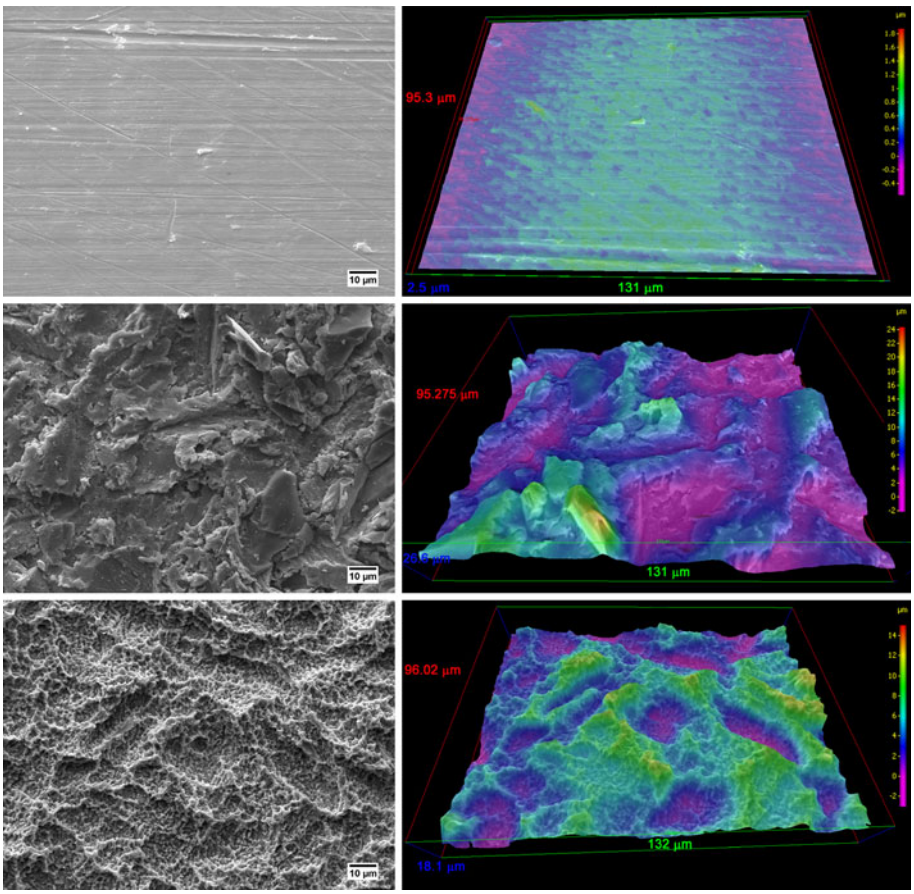

Fig. 1 Scanning electron micrographs in top view (*left row*) and false color 3D topographical scanning electron micrographs of M (*upper line*), SB (*middle line*), and SBA (*lower line*) Ti substrates

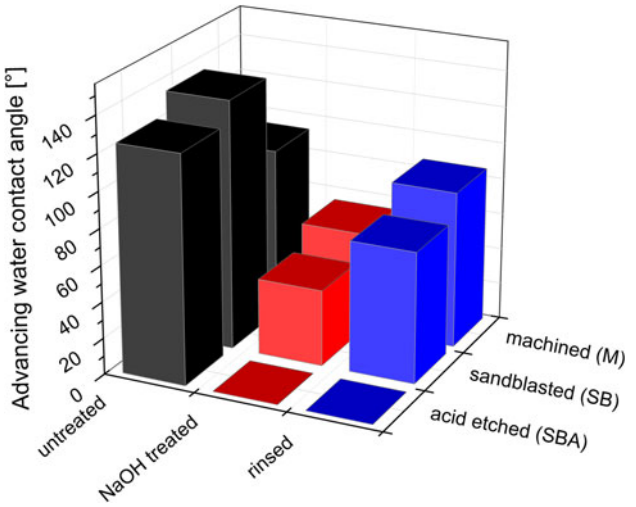

Fig. 2 Plot of the advancing water contact angles on M, SB, and SBA Ti substrates before alkali treatment, after alkali treatment and after alkali treatment and rinsing with deionized water. Values were obtained after drying the substrates and from the first immersion cycle

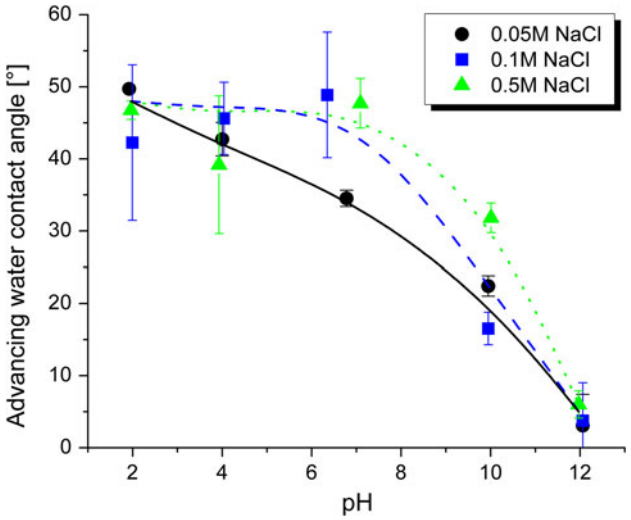

Fig. 3 Plot of the advancing water contact angle on SBA Ti substrates versus the pH of aqueous 0.05 M, 0.1 M, and 0.5 M sodium chloride solutions used for pretreatment. Values were obtained after drying the substrates and from the first immersion cycle

revealed that thermal acid etching effectively removed Al_2O_3 particles from the substrates.

Figure 2 shows the advancing water contact angles of M, SB, and SBA Ti substrates in the three different chemical states and indicates that surface roughness influenced the wetting behavior of the substrates in a different manner depending on the chemical state of the substrates. As evidenced by Fig. 2 the advancing water contact angles on untreated Ti substrates increased with increasing surface roughness from 90° on machined surfaces to 130° on the macrorough SB and 120° on the macro- and microrough SBA substrates. Untreated SB and SBA substrates could be clearly classified as hydrophobic and water repellent. Alkali treated and rinsed substrates by contrast showed water contact angles that decreased with increasing surface roughness, i.e., in the order M > SB > SBA. More specifically alkali treatment decreased the advancing water contact angles to 55° on M substrates, to 45° on the SB substrates and below 5° on the SBA substrates. The change in wettability upon alkali treatment was most pronounced for SBA substrates shifting the substrates from hydrophobic to superhydrophilic. Interestingly rinsing increased the advancing water contact angle of alkali treated M or SB substrates again to 90° and 70°, respectively, while the superhydrophilicity of alkali treated SBA substrates was fully preserved upon rinsing.

Hysteresis loops of the advancing and receding contact angles from subsequent immersion emersion cycles indicated that the hydrophobicity of untreated SBA substrates was metastable. More specifically advancing and receding contact angles of 0° were detected for the 2nd and following immersion emersion cycles of untreated SBA substrates. After drying the substrates the hydrophobic character of untreated SBA substrates was however fully restored while alkali treated or rinsed substrates retained their superhydrophilicity upon drying.

3.2 Influence of pH and ionic strength of treatment solutions on the wetting behavior of SBA substrates

The effect of pH and ionic strength of the treatment solution on the wetting behavior of SBA substrates was assessed by measuring the advancing water contact angles of cylindrical SBA Ti substrates after treatment with aqueous sodium chloride solutions of varying pH and concentration.

Figure 3 shows the plot of the advancing water contact angles on SBA substrates as a function of pH and concentration of the sodium chloride treatment solution. For all sodium chloride concentrations treatment with solutions of pH 7 or lower resulted in advancing contact angles between 35 and 50°. Above pH 7 however the advancing water contact angle decreased with increasing pH of the treatment solution. Treatment solutions of pH 12 yielded superhydrophilic SBA Ti substrates. The ionic strength had only an effect on the wetting behavior of SBA substrates between pH 7 and 12 and water contact angles decreased with decreasing ionic strength in this pH region.

3.3 XPS-characterization of alkali treated SBA substrates

The chemical composition of the topmost surface of individually treated SBA Ti substrates was characterized by

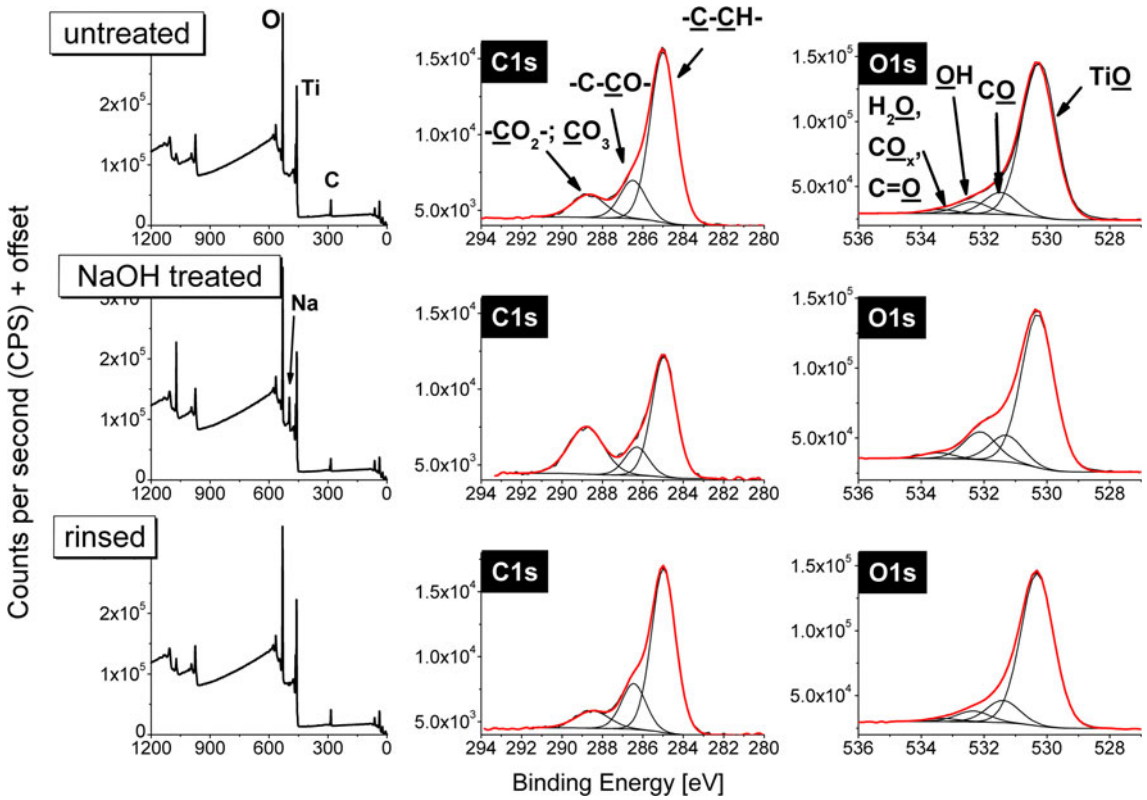

Fig. 4 Survey and deconvoluted high resolution C1s and O1s XPS spectra of untreated, alkali treated and of rinsed SBA Ti substrates

Table 2 Relative elemental compositions of untreated, alkali treated and alkali treated and rinsed SBA Ti substrates as derived from XPS survey spectra

Modification	Ti	O	C	Na
Untreated	24.5 ± 0.2%	55.3 ± 0.6%	20.2 ± 0.7%	n.d.
NaOH treated	20.7 ± 0.4%	51.0 ± 0.8%	17.2 ± 1.4%	11.1 ± 0.5%
Rinsed	24.4 ± 0.5%	54.2 ± 0.8%	20.7 ± 1.1%	0.9 ± 0.2%

Table 3 Relative elemental contributions to the C1s signal for untreated, alkali treated and alkali treated and rinsed SBA Ti substrates

Modification	C–CH	CO	CO_2, CO_3
Untreated	70.1 ± 1.2%	16.8 ± 0.6%	13.1 ± 0.7
NaOH treated	55.3 ± 1.9%	16.8 ± 4.0%	28.0 ± 3.0%
Rinsed	70.1 ± 0.5%	18.4 ± 0.7%	11.5 ± 0.8%

XPS. Figure 4 shows the survey and high resolution spectra of the C1s and O1s signals of untreated, alkali treated and of rinsed SBA Ti substrates and Tables 2, 3, 4 report the derived elemental compositions of the substrate surfaces.

The survey spectra of untreated SBA Ti substrates showed Ti, oxygen (O), and carbon (C) as main elements with an O/Ti ratio of 2.26 and a relative C content of 20%. After alkali treatment sodium (Na) signals Na1s and NaKLL at 1071 eV and 496 eV were detected, the O/Ti ratio increased to 2.5 and the relative C content decreased to 17%.

Table 4 Relative elemental contributions to the XPS O1s signal for untreated, alkali treated and alkali treated and rinsed SBA Ti substrates

Modification	TiO	C–O	OH	CO_x/H_2O
Untreated	78.0 ± 0.8%	11.6 ± 0.4%	7.7 ± 0.3%	2.7 ± 0.2%
NaOH treated	71.3 ± 0.4%	11.9 ± 0.6%	14.2 ± 1.1%	2.7 ± 0.4%
Rinsed	77.6 ± 2.0%	11.1 ± 1.6%	7.6 ± 0.9%	2.9 ± 0.2%

Contributions to the high resolution XPS C1s signals in Fig. 4 were allocated to aliphatic, ether and alcohol bound (CO) as well as to carboxylate (CO_2) and carbonate bound (CO_3) carbon and the derived atomic partial contributions of these species to the total C content are reported in Table 3. Individual contributions of CO_2 and CO_3 species were indicated by the relatively high full height at maximum width (FHMW) values that were required in the deconvolution routines but could not be further resolved. On untreated SBA substrates total C was detected as 70% aliphatic, 17% CO bound and 13% CO_2 or CO_3 bound C and after alkali treatment the corresponding values were shifted to 55% aliphatic, 17% CO bound, and 28% CO_2 and CO_3 bound C indicating a relative decrease in aliphatic and

a relative increase in CO_2 and CO_3 bound C. The increase of the latter species on alkali treated substrates might at least partly be attributed to carbonate formation during drying and storage of the substrates at ambient air.

XPS O1s high resolution spectra were deconvoluted as described by McCafferty et al. [41] by assigning the following contributions:

- Ti bound O^{2-} at 530.3 eV
- Oxygen bound to multiple carbon atoms (C–O–C species) at 531.0 eV
- TiO_{2-x} bound OH and OH^--ions at 532.0–532.5 eV
- Oxygen atoms multiple-bound to carbon (CO_x) and H_2O at 533.3 eV

Individual contributions from CO_x and water could not be resolved. On untreated SBA substrates oxygen was detected as 78% TiO_{2-x} bound, 11.6% C bound, 7.7% OH bound and 2.7% CO_x bound oxygen. After alkali treatment especially the fractions of TiO_{2-x} bound oxygen decreased to 71% and the one of OH bound oxygen increased to 14% while the peak maximum of the latter signal was shifted from 532.5 to 532 eV. This peak shift indicates an increased surface concentration of OH^- ions, which possess a higher electron density and therefore a lower binding energy compared to the OH groups of the TiO_{2-x} surface.

No significant differences between the XPS survey or high resolution spectra of rinsed and untreated SBA substrates were found except a residual relative Na content of 1% on the rinsed SBA substrates.

3.4 TOF-SIMS characterization of alkali treated SBA substrates

Chemical changes in the uppermost part of the SBA surface upon alkali treatment were followed by TOF-SIMS and Figs. 5 and 6 compare the spectra of positive and negative secondary ions of SBA Ti implants before and after alkali treatment.

Cationic fragments in positive mode TOF-SIMS of untreated SBA implants could be mainly attributed to hydrocarbons and TiO_{2-x} (Fig. 5). After alkali treatment the intensities of these hydrocarbon fragments decreased and mainly fragments of TiO_{2-x}, sodium hydroxide and sodium carbonate were detected. The overall sum of signal intensities of cationic secondary ions was also significantly reduced upon alkali treatment.

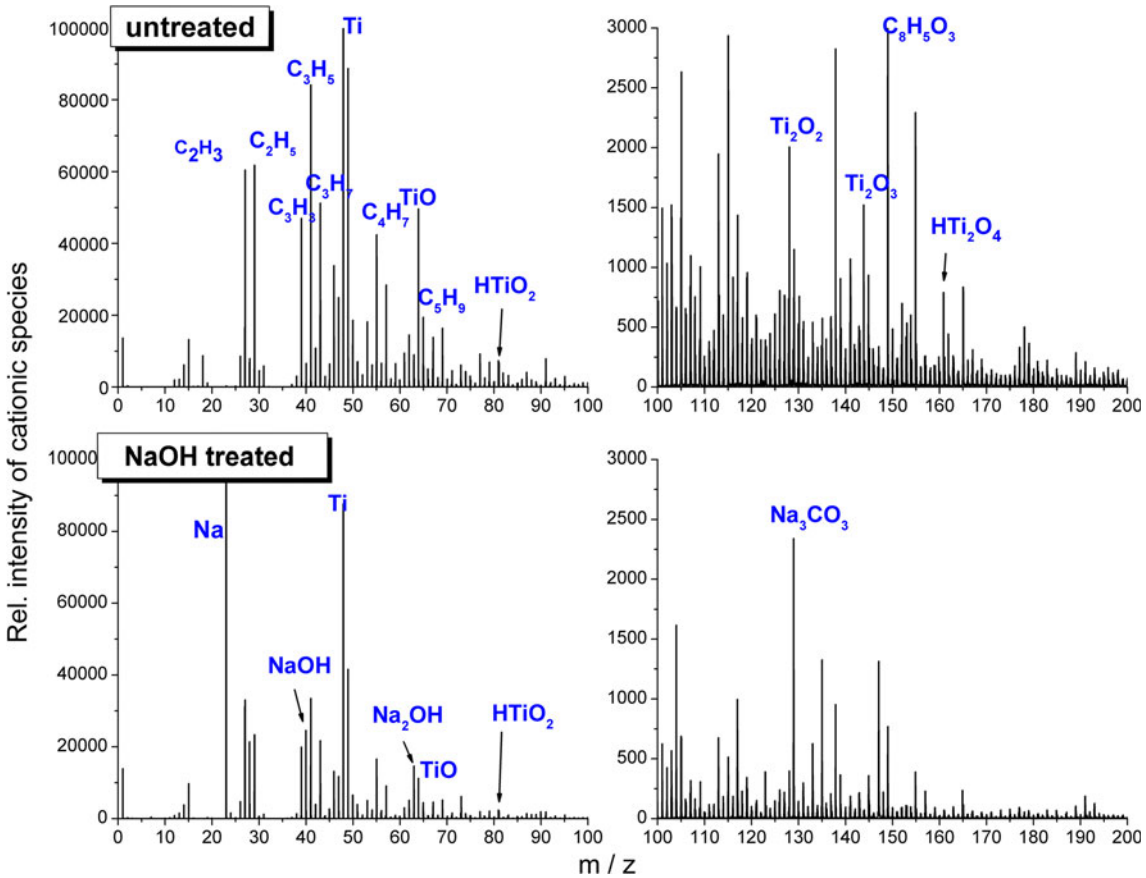

Fig. 5 Positive mode TOF–SIM spectra of commercial SBA Ti implants before and after alkali treatment

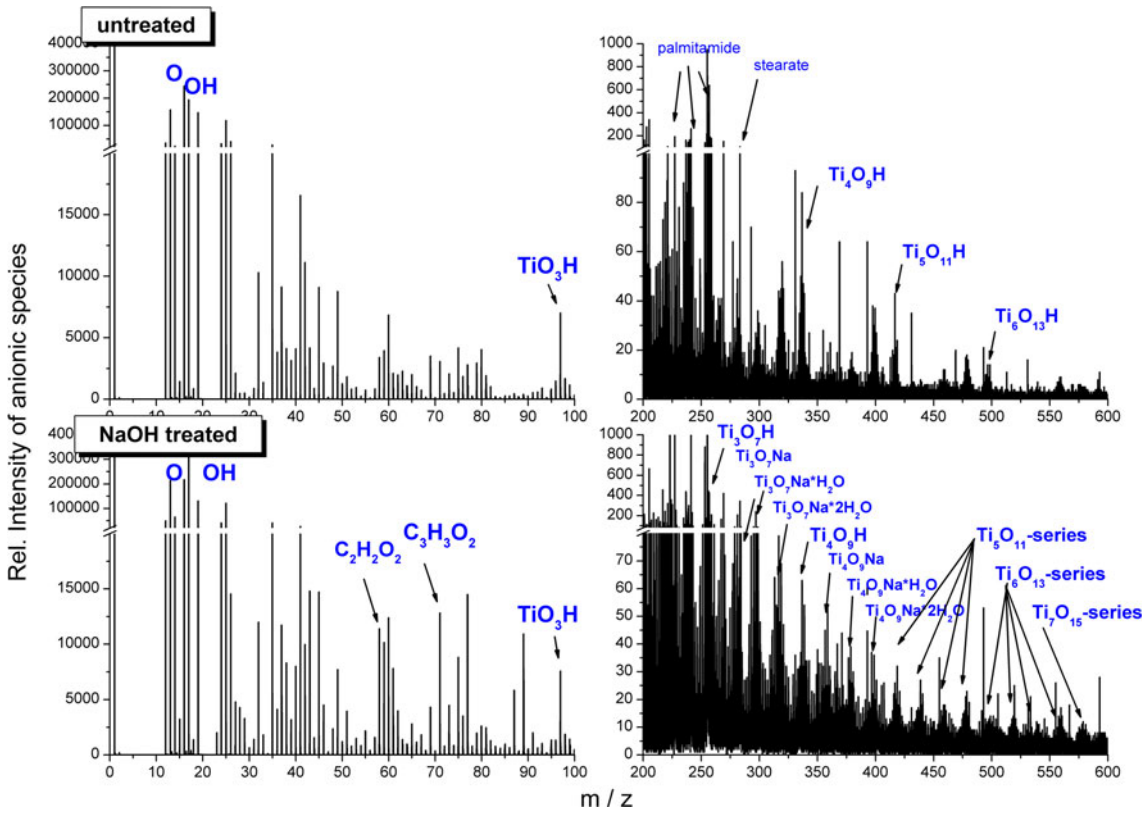

Fig. 6 Negative mode TOF–SIM spectra of commercial SBA Ti implants before and after alkali treatment

TOF-SIM spectra of anionic fragments of untreated and alkali treated SBA implants are shown in Fig. 6 and mainly consisted of fragments from hydrocarbons and TiO_{2-x}. Significant differences between the spectra of untreated and alkali treated samples were observed especially above 200 u and indicate a change of surface chemistry of the TiO_{2-x} surface upon alkali treatment. On untreated substrates mainly TiO_x cluster ions of the type $Ti_xO_{2x+1}H^-$ were detected. After alkali treatment however additional cluster ions of the form $Ti_xO_{2x+1}Na^-$ and of their hydrated analogues $Ti_xO_{2x+1}Na*mH_2O$ with x = 3, 4, 5, 6, and 7 and with m = 1 and 2 resulting in a series of regularly spaced signals were observed. The overall sum of intensities of anionic species was furthermore significantly increased after alkali treatment of SBA substrates and might indicate an increased negative charge on the surface of alkali treated SBA substrates.

3.5 Long-term properties of alkali treated SBA substrates

The evolution of the chemical surface composition and wetting properties of alkali treated SBA substrates upon storage at ambient conditions was assessed via time dependent XPS-, surface pH and wettability measurements.

Figure 7a and b show the evolution of the XPS derived fractions of total C and the relative contributions to the C1s signal, i.e., aliphatic, CO bound and CO_2 and CO_3 bound C species on alkali treated SBA substrates upon storage. The fraction of total C decreased from 20% before the treatment to a minimum of 15% after alkali treatment and 1 day of storage and subsequently increased again to a saturation value of 35–40% total C after 25 days of storage. Within the total C similarly aliphatic C decreased from 70% before the treatment to 55% directly after the alkali treatment and further to a minimum of 50% after 1 day of storage. Compared to total C aliphatic C increased faster upon further storage and leveled off in a saturation value of 60–65% already after 6 days. The fractions of CO_2 and CO_3 bound C on SBA substrates increased from 13% on the untreated substrates to a maximum of 32% after alkali treatment and 1 day of storage. Further storage however decreased the fractions of CO_2 and CO_3 bound C to an equilibrium value of ca. 20% after 14 days of storage. The increase in aliphatic and total as well as in CO_2 and CO_3 bound C on alkali treated SBA substrates upon storage might be attributed to CO_2 assimilation and carbonate formation as well as to a constant adsorption of mostly aliphatic organic contaminants from ambient atmosphere.

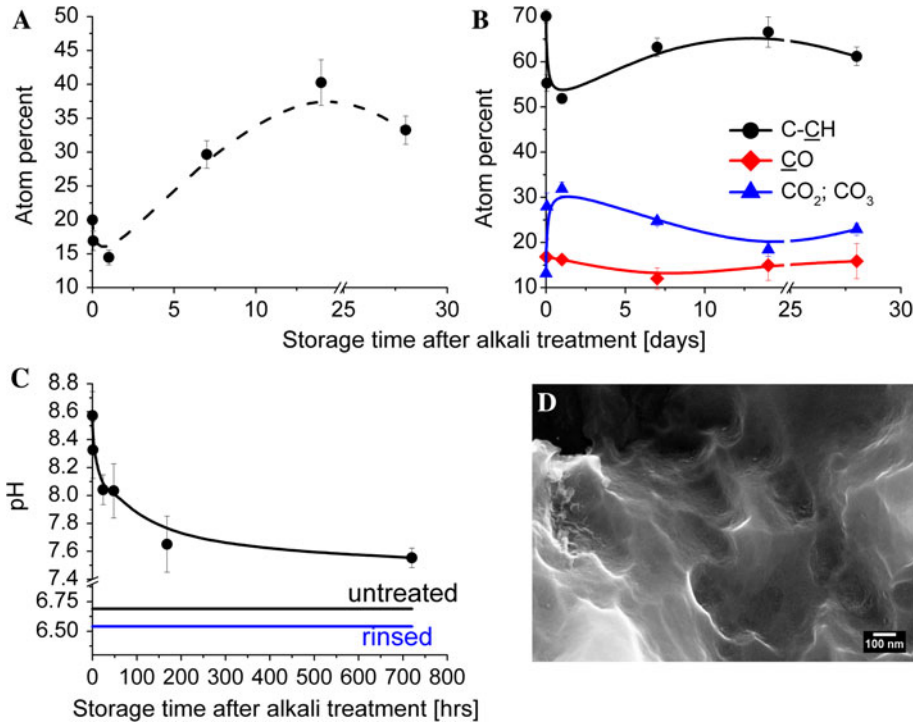

Fig. 7 Temporal evolution of the relative carbon content as derived from XPS (**a**) and of individual carbon species contributing to the XPS C1s signal (**b**) on alkali treated SBA Ti substrates upon storage. **c** Temporal evolution of surface pH as measured with a microelectrode on alkali treated SBA Ti substrates upon storage at ambient conditions. **d** SEM image of an alkali treated SBA Ti substrate in 180.000-fold magnification

The proposed sodium carbonate formation on alkali treated SBA substrates was further evidenced by the rapid drop of pH from 8.6 directly after alkali treatment to 7.6 after 7 days of storage (Fig. 7c). The latter value was significantly increased compared to the values of ca. 6.6 of untreated or rinsed surfaces respectively. The difference between the pH of the 0.05 M NaOH solution of 12.7 and the initial value of 8.6 that was measured on the substrate surface of SBA substrates directly after alkali treatment can be attributed to a dilution effect, which is linked to the chosen measurement technique.

As evidenced by the scanning electron micrograph in high magnification in Fig. 7d no deposits of sodium hydroxide or sodium carbonate were found on alkali treated SBA substrates. Furthermore, the topography of alkali treated SBA substrates did not significantly differ from the untreated substrates (not shown).

Long-term DCA measurements furthermore indicated that alkali treated SBA substrates remained superhydrophilic even after storage for several weeks (data not shown).

3.6 Fibrinogen Alexa Fluor conjugate adsorption

Protein adsorption experiments using a fluorescent fibrinogen Alexa Fluor 546 conjugate indicated qualitative and quantitative differences in the protein adsorption between alkali treated and untreated SBA substrates. Figure 8 shows a micrograph of the relative fluorescence intensities at a boundary between untreated and alkali treated SBA substrate regions after 5 min of incubation in a 1 μM solution of the fibrinogen conjugate and subsequent washing steps to remove residual non-adsorbed protein. While homogeneous protein films formed on the alkali treated SBA substrates protein films on untreated substrate regions were inhomogeneous and showed regions of up to 300 μm in diameter without protein and lacking any significant levels of fluorescence intensity. Digital image analysis of these inhomogeneous protein films on untreated SBA substrates further revealed a number average diameter of 20–30 μm for these protein free regions and a percentage of 15% of the untreated SBA surface that remained uncovered by protein. The determined average size of protein free regions correlated well with the size of the macro-cavities of the SBA surface.

Additionally line profiling of fluorescence intensities across the boundary between alkali treated and untreated zones in Fig. 8 revealed a mean relative fluorescence intensity of 120 a.u. on the untreated region and of 70 a.u. on the alkali treated zone indicating that fibrinogen adsorption was increased on untreated substrates compared to the alkali treated ones.

4 Discussion

4.1 Roughness induced wetting

The wetting behavior of untreated, alkali treated and rinsed M, SB, and SBA substrates reflects the empiric rule that hydrophilicity or hydrophobicity are each both enhanced

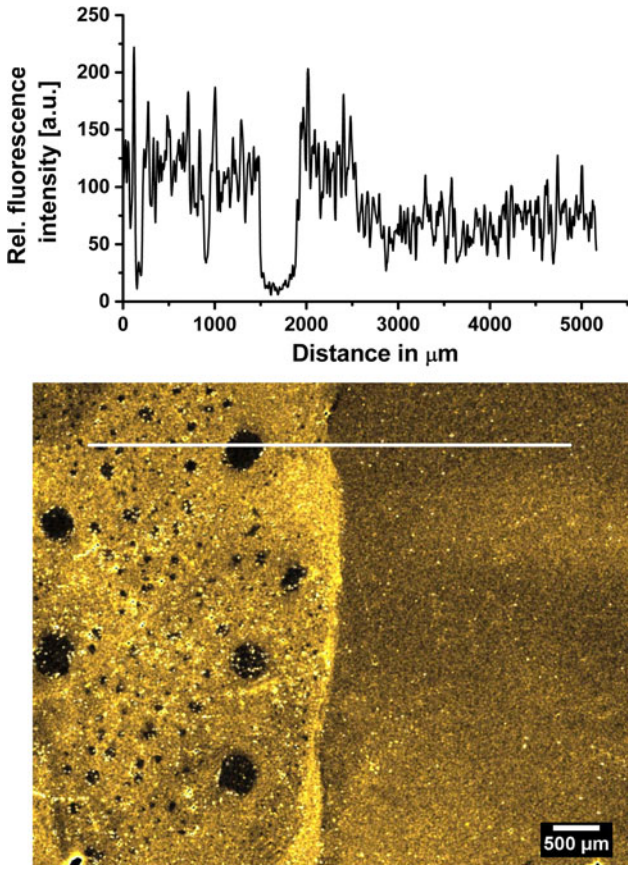

Fig. 8 Fluorescence micrograph of the border between untreated (*left*) and alkali treated (*right*) zones of a SBA Ti substrate after incubation in a 1 μM fibrinogen Alexa Fluor solution for 5 min and subsequent washing steps. The intensity profile was obtained from line scan (*white line*) across this border

with increasing Wenzel roughness [28]. For Ti substrates this tendency has been shown by Lim and Oshida [42]. The apparently contradictorily decrease of the advancing contact angles from untreated SB to SBA substrates might be influenced by the relatively high amounts of entrapped Al_2O_3 particles in SB substrates, which might render the wetting behavior of SB substrates more complex compared to M or SBA substrates.

Due to the relatively high contact angles and the complex surface topography of untreated SBA substrates wetting of these substrates most probably occurs via a Cassie-Baxter regime. In this regime contact lines of advancing droplets are supposed to pin to edges and spikes of the SBA surface and air is entrapped in (macro-)cavities of the SBA surface underneath the wetting liquid resulting in an incomplete contact between the liquid and the SBA surface. Wetting of alkali treated or rinsed SBA substrates is by contrast expected to result in a film regime. Here, the (macro)-cavities of the hydrophilic SBA substrates are supposed to fill with wetting liquid in front of the contact line of advancing droplets due to capillary forces. This process is described as hemi-wicking [28]. As a result the contact line of the wetting front that interacts with the substrate surface is supposed to be decreased and the wetting front of an advancing droplet is expected to contact mainly the advancing water film in the cavities of the substrate. Thus, this regime explains well the low water contact angles on alkali treated and rinsed SBA substrates. Furthermore, the assumption of a Cassie Baxter and a film regime for the wetting of untreated and alkali treated SBA substrates, respectively, are also indicated by the formation of inhomogeneous fibrinogen films on untreated and of homogeneous protein films on alkali treated SBA substrates.

4.2 Alkali treatment induced changes of chemical surface properties

The type and extent of chemical changes that are induced on TiO_{2-x} surfaces upon alkali treatment were reported to depend on the concentration, temperature and duration of the treatment [18–20, 26, 36, 43]. We think that the following observations are most relevant for the interpretation of the main chemical changes occurring on Ti SBA substrates upon alkali treatment: (1) Superhydrophilicity was only achieved after treatment with solutions of pH above the isoelectric point of TiO_{2-x}, i.e., above pH = 4–6 [44]. (2) XPS did not show any significant difference between untreated and rinsed substrates except a residual sodium signal on the rinsed SBA substrates. (3) TOF-SIMS spectra of alkali treated SBA substrates showed (hydrated) $Ti_xO_{2x+1}Na_y$-clusters. (4) The signal intensities of cationic species were decreased and those of anionic species were increased upon alkali treatment, which indicates an increase in negative surface charge upon alkali treatment.

As reported by Connor et al. the main processes occurring on the TiO_{2-x} surface under mild chemical conditions as upon the reported treatment with a 5 mM NaOH solution were protonation and deprotonation of terminal Ti–OH and oxo-bridged Ti–O–Ti groups [43]. By titrating TiO_2 particles with NaOH solutions Boehm et al. could furthermore show that proton exchange against Na^+ occurred on TiO_2 surfaces even at concentrations as low as 1 mM and that at NaOH concentrations of 0.05 M 70–75% of acidic OH-sites on the TiO_2 surface were deprotonated [45]. Harsher conditions by contrast were reported to result in partial dissolution of the TiO_{2-x} layer, sodium titanate hydrogel formation and a significant increase of the TiO_{2-x} layer thickness and were applied by, e.g., Von Wilmowsky et al. and Kim et al. who prepared superhydrophilic Ti substrates using 10 mM and 10 M NaOH solutions for 24 h at 60°C, respectively [18, 36].

Additionally to surface chemistry the extent of carbon contaminations on the TiO_{2-x} surface was also reported to influence the wetting properties of microrough Ti

substrates. Rupp et al. have, e.g., shown that storage of freshly prepared sandblasted and acid etched Ti substrates in sodium chloride solution (modSLA) effectively prevented contamination of Ti substrates and XPS carbon contents as low as 15% were reported for these superhydrophilic modSLA substrates while ca. 35% of carbon was found on the hydrophobic reference substrates (SLA) [31]. As reported by Connor et al. [43] adsorbed organic contaminations and carbonate were however also removed from the TiO_{2-x} surface by alkali treatment with 5 mM NaOH solution. These reports are consistent with our XPS results that have indicated a decrease of total and aliphatic carbon contents on SBA substrates upon alkali treatment. We think that the increased wetting of alkali treated and rinsed SBA substrates is however unlikely to be associated to a reduction of carbon contaminations since carbon contents on hydrophobic untreated and superhydrophilic rinsed SBA Ti substrates were comparable and were ca. 20% for both mentioned substrate types.

With respect to the mild conditions of the here applied alkali treatment protocol and concluding from the comparison with the reported literature we assume that deprotonation of terminal Ti–OH and oxo-bridged Ti–OH–Ti groups and ion exchange leading to the formation of $Ti–O^{-}Na^{+}$ ion pairs might be the most important chemical changes for the here presented alkali treatment of SBA Ti substrates. Although especially the TOF–SIM spectra might also suggest a partial dissolution of the TiO_{2-x} layers and sodium titanate formation as reported for the treatment under harsh chemical conditions [18] the lack of significant differences between XPS spectra of untreated and rinsed SBA Ti substrates omitted any quantification of these processes on the here described alkali treated SBA Ti substrates.

4.3 Protein adsorption

The decreased adsorption of fibrinogen Alexa Fluor conjugate on superhydrophilic alkali treated SBA Ti substrates correlates well the general tendency of fibrinogen and other adhesion proteins to adsorb preferentially on hydrophobic substrates compared to hydrophilic ones. Nygren et al., e.g., have shown that fibrinogen adsorption on hydrophilic quartz substrates was decreased by 30% compared to hydrophobic quartz substrates [46] and Nygren further reported that compared to hydrophilic titanium substrates the amount of adsorbed fibrinogen from whole blood was twofold increased on hydrophobic reference substrates [47].

In addition to the influence of surface hydrophilicity Michael et al. have analyzed the effect of surface charge on protein adsorption [48] and reported that fibronectin fragment $FNIII_{7–10}$ adsorption increased in the order of the following surface characteristics: "positively charged"> "hydrophobic" > "negatively charged" > "hydrophilic". The decreased fibrinogen adsorption on superhydrophilic and hypothetically negatively charged alkali treated SBA Ti substrates is in good agreement with this sequence. Interestingly modSLA surfaces were reported to be positively charged and compared to hydrophobic SLA substrates an increased fibronectin adsorption was reported on modSLA substrates [49].

4.4 General discussion and context to osseointegration

From a surface-chemical perspective downstream host responses to implanted materials as osseointegration are linked to the physicochemical properties of the implant surface by a sequence of ion adsorption, ion exchange, protein adsorption, cell interrogation, mineralization, and remodeling [2]. In this sequence especially the characteristics of the adsorbing protein film are believed to directly determine cell and tissue processes and hence link the physicochemical properties of implanted materials to the physiological response of the host. The amount and conformational state of adsorbed fibrinogen, e.g., has been used as a biocompatibility indicator of artificial surfaces [50] and the amount of denatured fibrinogen, which accumulates on implant surfaces was correlated with the extent of biomaterial-mediated inflammation [51]. At the same time fibrinogen itself has been reported to show a higher tendency to denature on hydrophobic surfaces compared to hydrophilic ones [23, 48]. These relations and our results suggest that the enhanced osseointegration of alkali treated SBA Ti implants might be linked to an alteration of the status of the protein film on the surface of these implants.

In addition to cell-physiological processes the physicochemical properties of the implant surface might also affect osseointegration by influencing the mineralizing capabilities of the implant surface. The importance of the nucleating and mineralizing properties of the implant surface is evidenced by the presence of thin mineralized interfacial transition layers between bone and osseointegrated implants [2, 52]. These afibrillar apatite-like layers probably result from acellular and surface induced mineralization and model studies indicate that adsorbing proteins might influence their formation by masking the nucleating sites of the TiO_{2-x} surface. Adsorbed fibronectin, e.g., was reported to inhibit the nucleation and mineralization of the TiO_{2-x} surface of Ti substrates upon incubation in Hanks' balanced salt solution suggesting that surfaces with decreased protein affinity might favor nucleation and mineralization [53]. The decreased protein affinity of alkali treated SBA substrates suggests that the enhanced osseointegrative potential of these substrates might therefore be also linked to enhanced mineralizing capabilities of this surface type. This subject will be addressed in future studies.

5 Conclusion

In this paper, we have demonstrated the preparation of superhydrophilic microrough titanium substrates by a rapid and convenient alkali treatment under mild chemical conditions. The chemical composition of the titanium surface was only marginally changed by reversible deprotonation and ion exchange processes upon alkali treatment and roughness induced wetting greatly contributes to the superhydrophilicity of alkali treated microrough Ti substrates. Qualitative and quantitative differences in protein adsorption between untreated and alkali treated substrates were however observed and might help to explain the enhanced osseointegration of superhydrophilic alkali treated microrough Ti implants. Due to its simplicity and biocompatibility the here presented alkali treatment can be regarded as an attractive clinically applicable route to render microrough Ti substrates superhydrophilic in situ of implantation without the necessity to modify production and storage routines of the implants.

Acknowledgments The authors are grateful to Prof. Uwe Pieles and Theo Bühler (FHNW Muttenz, Switzerland) for technical support of this study.

References

1. Albrektsson T, Brånemark PI, Hansson HA, Lindström J. Osseointegrated titanium implants. Acta Orthop Scand. 1981;52:155–70.
2. Puleo DA, Nanci A. Understanding and controlling the bone-implant interface. Biomaterials. 1999;20:2311–21.
3. Kasemo B. Biocompatibility of titanium implants: surface science aspects. J Prosthet Dent. 1983;49:832–7.
4. Albrektsson T, Wennerberg A. Oral implant surfaces: part 1—review focusing on topographic and chemical properties of different surfaces and in vivo responses to them. Int J Prosthodont. 2004;17:536–43.
5. Le Guéhennec L, Soueidan A, Layrolle P, Amouriq Y. Surface treatments of titanium dental implants for rapid osseointegration. Dent Mater. 2007;23:844–54.
6. Wennerberg A, Albrektsson T, Andersson B, Krol JJ. A histomorphometric and removal torque study of screw-shaped titanium implants with three different surface topographies. Clin Oral Impl Res. 1995;6:24–30.
7. Wennerberg A, Hallgren C, Johansson C, Danelli S. A histomorphometric evaluation of screw-shaped implants each prepared with two surface roughnesses. Clin Oral Impl Res. 1998;9:11–9.
8. Cooper LF. A role of surface topography in creating and maintaining bone at titanium endosseous implants. J Prosth Dent. 2000;84:522–34.
9. Davies JE. Understanding peri-implant endosseous healing. J Dent Edu. 2003;67:932–49.
10. Martin JY, Schwartz Z, Hummert TW, Schraub DM, Simpson J, Lankford J, Dean DD, Cochran DL, Boyan BD. Effect of titanium surface roughness on proliferation, differentiation, and protein synthesis of human osteoblast-like cells (MG 63). J Biomed Mater Res. 1995;29:389–401.
11. Lossdörfer B, Schwartz Z, Wang L, Lohmann CH, Turner JD, Wieland M, Cochran DL, Boyan BD. Microrough implant surface topographies increase osteogenesis by reducing osteoclast formation and activity. J Biomed Mater Res. 2004;70A:361–9.
12. Pilliar RM. Implant surface design for development and maintenance of osseointegration. In: Ellingson JE, Lyngstadaas SP, editors. Bio-implant interface. Boca Raton: CRC press; 2003. p. 43–58.
13. Franchi M, Fini M, Giavaresi G, Ottani V. Peri-implant osteogenesis in health and osteoporosis. Micron. 2005;36:630–44.
14. Keselowsky BG, Collard DM, Garcìa AJ. Integrin binding specificity regulates biomaterial surface chemistry effects on cell differentiation. Proc Natl Acad Sci USA. 2005;102:5953–7.
15. Zhao G, Schwartz Z, Wieland M, Rupp F, Geis-Gerstorfer J, Cochran DL, Boyan BD. High surface energy enhances cell response to titanium substrate microstructure. J Biomed Mater Res. 2005;74A:49–58.
16. Buser D, Broggini N, Wieland M, Schenk RK, Denzer AJ, Cochran DL, Hoffmann B, Lussi A, Steinemann SG. Enhanced bone apposition to a chemically modified SLA titanium surface. J Dent Res. 2004;83:529–33.
17. Ferguson SJ, Broggini N, Wieland M, de Wild M, Rupp F, Geis-Gerstorfer J, Cochran DL, Buser D. Biomechanical evaluation of the interfacial strength of a chemically modified sandblasted and acid-etched titanium surface. J Biomed Mater Res. 2006;78A:291–7.
18. Kim HM, Miyaji F, Kokubo T, Nakamura T. Preparation of bioactive Ti and its alloys via simple chemical surface treatment. J Biomed Mater Res. 1996;32:409–17.
19. Takadama T, Kim HM, Kokubo T, Nakamura T. An X-ray photoelectron spectroscopy study of the process of apatite formation on bioactive titanium metal. J Biomed Mater Res. 2001;55:185–93.
20. Jonášovà L, Müller F, Helebrant A, Strnad J, Greil P. Biomimetic apatite formation on chemically treated titanium. Biomaterials. 2004;25:1187–94.
21. Vroman L. The life of an artificial device in contact with blood: initial events and their effect on its final state. Bull N Y Acad Med. 1988;64:352–7.
22. Olivares-Navarette R, Raz P, Zhao G, Chen J, Wieland M, Cochran DL, Chaudhri RA, Ornoy A, Boyan BD, Schwartz Z. Integrin $\alpha 2\beta 1$ plays a critical role in osteoblast response to micron-scale surface structure and surface energy of titanium substrates. Proc Natl Acad Sci USA. 2008;105:15767–72.
23. Roach P, Farrar D, Perry CC. Interpretation of protein adsorption: surface-induced conformational changes. J Am Chem Soc. 2005;127:8168–73.
24. Vroman L, Adams AL, Fischer GC, Munoz PC. Interaction of high molecular weight kininogen in plasma at interfaces. Blood. 1980;55:156–9.
25. Textor M, Sitting C, Frauchiger V, Tosatti S, Brunette DM. Properties and biological significance of natural oxide films on titanium and its alloys. In: Brunette DM, Tengvall P, Textor M, Thomsen P, editors. Titanium in medicine. Berlin: Springer; 2001. p. 172–224.
26. Kokubo T, Kim HM, Kawashita M. Novel bioactive materials with different mechanical properties. Biomaterials. 2003;24:2161–75.
27. Rupp F, Scheideler L, Olshanska N, de Wild M, Wieland M, Geis-Gerstorfer J. Enhancing surface free energy and hydrophilicity through chemical modification of microstructured titanium implant surfaces. J Biomed Mater Res. 2006;76A:323–34.
28. Bico J, Thiele U, Quéré D. Wetting of textured surfaces. Colloids Surf A Physicochem Eng Aspect. 2002;206:41–6.

29. Ameen AP, Short RD, Johns R, Schwach G. The surface analysis of implant materials. The surface composition of a titanium dental implant material. Clin Oral Impl Res. 1993;4:144–50.
30. Massaro C, Rotolo P, De Riccardis F, Milella E, Napoli A, Wieland M, Textor M, Spencer ND, Brunette DM. Comparative investigation of the surface properties of commercial titanium dental implants. Part I: chemical composition. J mater sci mater med. 2002;13:535–48.
31. Rupp F, Scheideler L, Rehbein D, Axmann D, Geis-Gerstorfer J. Roughness induced dynamic changes of wettability of acid etched titanium implant modifications. Biomaterials. 2004;25:1429–38.
32. Aita H, Hori N, Takeuchi M, Suzuki T, Yamada M, Anpo M, Ogawa T. The effect of ultraviolet functionalization of titanium on integration with bone. Biomaterials. 2009;30:1015–25.
33. Baier RE, Meyer AE. Future directions in surface preparation of dental implants. J Dent Ed. 1988;52:788–91.
34. Feng B, Weng J, Yang BC, Qu SX, Zhang XD. Characterization of surface oxide films on titanium and adhesion of osteoblasts. Biomaterials. 2003;24:4663–70.
35. Jennissen HP. Ultra-hydrophilic transition metals as histophilic biomaterials. Macromol Symp. 2005;225:43–69.
36. Von Wilmowsky C, Müller L, Lutz R, Lohbauer U, Rupp F, Neukam FW, Nkenke E, Schlegel KA, Müller FA. Osseointegration of chemically modified titanium surfaces: an in vivo study. Adv Eng Mater. 2008;10:B61–6.
37. Stadlinger B, Lode A, Eckelt U, Range U, Schlottig F, Hefti T, Mai R. Surface-conditioned dental implants: an animal study on bone formation. J Clin Periodont. 2009;36:882–91.
38. Stadlinger B, Mai R, Lode AT, Eckelt U. Evaluation of surface conditioned dental implants–an animal study. Int J Oral Maxillofac Surg. 2009;38:454.
39. Whitehouse DJ. Handbook of surface metrology. London: Institute of Physics Publishing; 1994.
40. Wieland M, Textor M, Spencer ND, Brunette DM. Wavelength-dependent roughness: a quantitative approach to characterizing the topography of rough titanium surfaces. Int J Oral Maxillofac Implants. 2001;16:163–81.
41. McCafferty E, Wightman JP. Determination of the concentration of surface hydroxyl groups on metal oxide films by a quantitative XPS method. Surf Interface Anal. 1998;26:549–64.
42. Lim YJ, Oshida Y. Initial contact angle measurements on variously treated dental medical titanium materials. Bio-Med Mater Eng. 2001;11:325–41.
43. Connor PA, Dobson KD, McQuillan AJ. Infrared spectroscopy of the TiO_2/aqueous solution interface. Langmuir. 1999;15:2402–8.
44. Schliephake H, Scharnweber D. Chemical and biological functionalization of titanium for dental implants. J Mater Chem. 2008;18:2404–14.
45. Boehm HP. Acidic and basic properties of hydroxylated metal oxide surfaces. Discuss Faraday Soc. 1971;52:264–75.
46. Nygren H, Stenberg H, Karlsson C. Kinetics supramolecular structure and equilibrium properties of fibrinogen adsorption at liquid-solid interfaces. J Biomed Mater Res. 1992;26:77–91.
47. Nygren H. Initial reactions of whole blood with hydrophilic and hydrophobic titanium surfaces. Coll Surf B Bioint. 1996;6:329–33.
48. Michael KE, Vernekar VN, Keselowsky BG, Meredith JC, Latour RA, García AJ. Adsorption–induced conformational changes in fibronectin due to interactions with well-defined surface chemistries. Langmuir. 2003;19:8033–40.
49. Scheideler L, Rupp F, Wieland M, Geis-Gerstorfer J. Storage conditions of titanium implants influence molecular and cellular interactions; 83rd general session and exhibition of the international association for dental research; 2006. Poster # 870.
50. Salzman EW, Linden J, McManama G, Ware JA. Role of fibrinogen in activation of platelets by artificial surfaces. Annals NY Acad Sci. 1987;516:184–95.
51. Tang L, Wu Y, Timmons RB. Fibrinogen adsorption and host tissue responses to plasma functionalized surfaces. J Biomed Mater Res. 1998;42:156–63.
52. Palmquist A, Jarmar T, Emanuelsson L, Brånemark R, Engqvist H, Thomsen P. Forearm bone-anchored amputation prosthesis: A case study on the osseointegration. Acta Orthop. 2008;79:78–85.
53. Serro AP, Fernandes AC, Saramago BJ. Calcium phosphate deposition on titanium surfaces in the presence of fibronectin. Biomed Mater Res. 2000;49:345–52.